Efficient numerical solver of the steady state thermohydrodynamic Reynolds equation for journal bearings

Silun Zhang[a,b], Mohamed-Amine Hassini[a], Mihai Arghir[b]

a. ERMES-IMSIA, EDF Lab Paris-Saclay, 91120 Palaiseau, France
b. PPRIME Institute, UPR CNRS 3346, Université de Poitiers, ISAE ENSMA, 86962 Chasseneuil Futuroscope, France
Corresponding author: silun-s.zhang@edf.fr

Résumé:

Lors d'une analyse en régime ThermoHydroDynamique (THD) dans le domaine de la lubrification, l'équation de Reynolds et l'équation de l'énergie doivent être couplées pour obtenir de manière précise les distributions de pression et de température. La résolution de ces équations couplées dans les paliers hydrodynamiques est accompagnée des phénomènes de cavitation et de turbulence dans le contexte d'un régime transitoire. A cause de la dépendance entre température et viscosité, cette résolution devient non-linéaire et très couteuse en termes du temps. Par conséquent, une méthode numérique efficace, nommée la méthode de colocation aux points Lobbato (LPCM), est présentée dans cet article. Le calcul d'un patin incliné 1D utilisant cette méthode montre la réduction considérable du temps de calcul par rapport à la méthode de résolution classique. Puis, cette méthode numérique intègre deux modèles de cavitation et est appliquée à un patin parabolique. Enfin, les données d'essai dans la littérature d'un palier à géométrie fixe avec deux lobes sont utilisées pour valider la méthode d'un point de vue expérimental.

Abstract:

State of the art analyses of oil-lubricated journal bearings requires numerical solution of the Reynolds equation coupled with the energy transport equation. Generally, for a journal bearing, the resolution of these coupled equations must include cavitation (film rupture and reformation), turbulent flow regime and transient (unsteady) operating conditions. Furthermore, due to the temperature-dependent viscosity, the coupled system becomes non-linear and time-consuming. Thus, in this paper, a spectral approach named Lobatto Point Collocation Method (LPCM) is presented. The combination of LPCM with two different film rupture/reformation models is validated using numerical results published in the literature in the cases of 1D slider. The substantial reduction of the computational time is highlighted compared to the Natural Discretization Method (NDM). The model predictions are also compared to the pressure and temperature distributions measured experimentally in the case of a two lobes journal bearing.

Keywords: steady ThermoHydroDynamic (THD) analysis, Cavitation Model, Lobatto point quadrature

1 Introduction

In fluid hydrodynamic bearings with low loads and low rotational speeds, the pressure field in the fluid film may be described by the classical isothermal Reynolds equation. However, for higher loads and higher rotational speeds, the isothermal approach is no longer sufficient and the variation of viscosity with temperature must be taken into account to obtain accurate predictions. Therefore, Reynolds and energy equations have to be coupled and solved sequentially. Besides, the energy equation must be discretized across the thin fluid film. The number of discretization points in this direction has to be large enough to capture the wall temperature gradients. For the turbulent flow regime, where these gradients are much steeper, the number of discretization points across the film is at least one order of magnitude larger than the one used in laminar flow conditions. Thus, the resolution of the coupled equations is very time consuming especially in the case of transient analysis. Although the numerical solution of these coupled equations is a solved problem since many decades, efficient numerical methods aimed to reduce the calculation effort are still to be developed.

In 1986, based on a Galerkin approach, Elrod and Brewe [1] developed a numerical reduction approach to solve the Reynolds equation coupled with the 2D energy equation with Dirichlet boundary conditions. Temperature and fluidity (inverse of viscosity) are approximated by third order Legendre polynomials across the fluid film thickness. Elrod used Lobatto point quadrature method to discretize and calculate the integral quantities across the film thickness. The pressure and temperature are discretized using the classical finite difference methods in the other directions. The method showed good agreement with classical approaches. In a subsequent work [2], Elrod improved the precision of the method by approximating the temperature and the fluidity using arbitrary orders Legendre polynomials. In 2005, Moraru [3] extends the approach presented by Elrod [2] to compressible fluids and takes also into account a temperature-dependent density. In his work, a 2D formulation of the energy equation neglecting the axial heat conduction is used. In contrast to [1] and [2], the density is also approximated by Legendre polynomials across the fluid film thickness. The governing partial differential equations are solved by finite difference methods with upwind scheme for numerical stability. In 2009, Feng and Kaneko [4] used the same approach as Moraru to calculate the temperature and the pressure distributions in a multi-wound foil bearing while taking into account foil deflections. Unlike Moraru, Feng and Kaneko solved the energy equation on a 3D computational domain using finite difference methods. In 2015, Mahner et al. [5] used the reduction approach to analyze steady state performances of thrust and slider bearings operating with a compressible fluid. The authors used the Quadrature Method, the Modified Quadrature Method, Lobatto Point Collocation Method and the Galerkin Method in order to reduce number of unknowns of the discretized equations. According to the authors, all these methods yielded a significant time reduction compared to the classical methods.

The aim of the present work is to develop an efficient and accurate numerical solver for the THD analysis of hydrodynamic bearings. Compared to the previous published studies, the present solver uses LPCM and takes into account the cavitation phenomenon (film rupture and reformation) which is tackled using two different approaches: the free boundary formulation of the incompressible Reynolds equation and the artificial compressibility approach. Besides, the coupled governing partial differential equations are solved using finite volume method and the solver is tested and validated against both numerical and experimental results in the literature.

2 Theoretical analysis

When taking into account the temperature-dependent viscosity, it is mandatory to solve sequentially the generalized Reynolds equation and the energy equation to obtain accurate pressure and temperature distributions in the fluid film.

2.1 Generalized Reynolds Equation with cavitation

For a journal bearing where the wall velocities are $u(x,h,z) = U$ and $u(x,0,z) = 0$, the generalized Reynolds equation writes [9] :

$$\frac{\partial}{\partial x}\left(G\frac{\partial p}{\partial x}\right) + \frac{\partial}{\partial z}\left(G\frac{\partial p}{\partial z}\right) = -U\frac{\partial(F)}{\partial x} \qquad \textbf{Eq.1}$$

where

$$G = \rho\left[\int_0^h I_1 d\xi - \frac{J_1}{J_0}\int_0^h I_0 d\xi\right] \;\; ; \;\; F = \rho\frac{\int_0^h I_0 d\xi}{J_0} \qquad \textbf{Eq.2}$$

$$I_0 = \int_0^y \frac{1}{\mu} d\xi \; ; \; I_1 = \int_0^y \frac{\xi}{\mu} d\xi \; ; J_0 = \int_0^h \frac{1}{\mu} d\xi \; ; \; J_1 = \int_0^h \frac{\xi}{\mu} d\xi \qquad \textbf{Eq.3}$$

Two approaches were used in the present work for the film rupture and reformation.

The first approach is based on the classical free boundary formulation of the incompressible Reynolds equation. It uses Jakobsson, Floberg and Olsson (JFO) cavitation model, implemented by Elrod and Adams [6], and assumes that the density in full film region is constant and that the pressure is equal to the cavitation pressure in the ruptured zone. The key point of JFO model is a filling fraction $\theta \in [0,1]$ for taking into account the effective density in the ruptured film zone. The $p-\theta$ formulation of JFO model is:

$$\frac{\partial}{\partial x}\left(G\frac{\partial p}{\partial x}\right) + \frac{\partial}{\partial z}\left(G\frac{\partial p}{\partial z}\right) = -U\frac{\partial[(1-\theta)F]}{\partial x} \qquad \textbf{Eq.4}$$

In 2015, Woloszynski et al. [7] used an efficient algorithm, called Fischer-Burmeister-Newton-Schur (FBNS), for solving the JFO model under the complementary constraint $(p - p_{cavi})\theta = 0$ in two-steps. This algorithm was integrated in the current solver.

The second method is based on an artificial compressibility model (ACM) that modifies the density of the lubricant in the cavitation region. Instead of using a mathematical constraint $(p - p_{cavi})\theta = 0$, this approach assumes that the fluid film is a homogenous mixture and that the density is a pressure-dependent thermodynamic variable. The density in cavitation region is a combination of gas density ρ_g and lubricant density ρ_l:

$$\rho = (1-\theta)\rho_l + \theta\rho_g \qquad \textbf{Eq.5}$$

The faction θ in Eq.5 has the same role as θ in JFO model. If the faction is zero ($\theta = 0$) there is no cavitation and the fluid film is complete. If $0 < \theta \leq 1$, film rupture is present and the fluid film is a homogenous mixture of lubricant and gas. In order to avoid abrupt transitions between ruptured and full film zones, θ is calculated by a regularized pressure-based law (Eq.6). The regularization is performed using the coefficient β:

$$\theta(p) = 1 - \frac{1}{1 + exp[-\beta(p - p_{cavi})]} \qquad \textbf{Eq.6}$$

2.2 3D Energy equation

The temperature distribution in the lubricant is described by the following energy equation [9]:

$$\underbrace{\rho C_p\left(u\frac{\partial T}{\partial x}+v\frac{\partial T}{\partial y}+w\frac{\partial T}{\partial z}\right)}_{convection}=\underbrace{\frac{\partial}{\partial y}\left(\lambda\frac{\partial T}{\partial y}\right)}_{conduction}+\underbrace{\mu\left[\left(\frac{\partial u}{\partial y}\right)^2+\left(\frac{\partial w}{\partial y}\right)^2\right]}_{dissipation} \qquad \textbf{Eq.7}$$

In the ruptured film region, the fluid is supposed to be a homogenous mixture. The heat capacity, thermal conductivity and viscosity are given as [9]:

$$\rho C_p=(1-\theta)\rho C_{p_l}+\theta\rho C_{p_g}$$
$$\lambda=(1-\theta)\lambda_l+\theta\lambda_g\ ;\ \mu=(1-\theta)\mu_l+\theta\mu_g \qquad \textbf{Eq.8}$$

The temperature-dependent viscosity of the liquid phase follows an exponentially decaying law:

$$\mu(T)=\ \mu_0 e^{-\alpha(T-T_0)} \qquad \textbf{Eq.9}$$

where μ_0 is the dynamic viscosity at the reference temperature T_0 and α is a given coefficient.

2.3 Formulation of the equations using LPCM

The Lobatto Point Collocation Method (LPCM) uses Legendre polynomials to approximate the temperature across the film thickness. Furthermore, the method simplifies the computation of the Dowson integrals (Eq.2 and Eq.3) in the generalized Reynolds equation. Because Legendre polynomials are defined on$[-1,1]$, the following coordinate transformation is used:

$$y=\frac{(\zeta+1)h}{2} \qquad \textbf{Eq.10}$$

Since the pressure is constant across the film thickness, the generalized Reynolds equation remains the same (i.e. Eq.1). Following the coordinate transformation, the energy equation (Eq.7) becomes:

$$u\frac{\partial T}{\partial x}+\frac{2}{h}\left[v-u\frac{(\zeta+1)}{h}\frac{\partial h}{\partial x}-w\frac{(\zeta+1)}{h}\frac{\partial h}{\partial z}\right]\frac{\partial T}{\partial\zeta}+w\frac{\partial T}{\partial z}$$
$$=\frac{\lambda}{\rho C_p}\frac{4}{h^2}\frac{\partial^2 T}{\partial\zeta^2}+\frac{\mu}{\rho C_p}\frac{4}{h^2}\left[\left(\frac{\partial u}{\partial\zeta}\right)^2+\left(\frac{\partial w}{\partial\zeta}\right)^2\right] \qquad \textbf{Eq.11}$$

For an incompressible lubricant, only the temperature T and the fluidity ξ_F (the inverse of the viscosity μ), are approximated across the film thickness (Eq.12).

$$\xi_F(x,\zeta_i,z)=\frac{1}{\mu(x,\zeta_i,z)}=\sum_{j=0}^{N}\widehat{\xi_F}_j(x,z)P_j(\zeta_i)\ \ ;\quad T(x,\zeta_i,z)=\sum_{j=0}^{N}\hat{T}_j(x,z)P_j(\zeta_i) \qquad \textbf{Eq.12}$$

Where $P_j(\zeta_i)$ is the jth order Legendre polynomial, N is its maximum order. $\widehat{\xi_F}_j(x,z)$, respectively $\hat{T}_j(x,z)$, are the polynomial coefficients of fluidity and temperature, respectively. The N+1 polynomial coefficients $\widehat{\xi_F}_j$ and $\hat{T}_j$ are calculated by applying the collocation method at N+1 Lobatto points ([3], [4]). These points are the *N-1* internal Lobatto points (i.e. the roots of $dP_N/d\zeta$) and the two boundary points $\zeta=-1$ and $\zeta=1$.

Compared to the Natural Discretization Method (NDM) which computes the temperature by solving the 3D energy equation discretized over the film thickness, the LPCM calculates the polynomial coefficients

of temperature $\widehat{T}_j$. For a given (x, z) position, the temperature in Eq.11 is replaced by its decomposition (i.e. Eq.12) for each internal Lobatto $\zeta = \zeta_i\,, i \in [1, \dots, N-1]$ across the fluid film leading to a partial differential equations with the N+1 unknown $\hat{T}_j$. The boundary conditions are applied at $\zeta = -1$ and $\zeta = 1$. The Dirichlet boundary condition at the journal surface T_0 and the Neumann boundary condition ϕ_q at the bearing are implemented by setting:

$$T_0 = T(x, 1, z) = \sum_{j=0}^{N} P_j(1)\hat{T}_j(x, z) \qquad \textbf{Eq.13}$$

$$\phi_q = \left.\frac{\partial T}{\partial \zeta}\right|_{\zeta=-1} = \sum_{j=0}^{N} \left.\frac{\partial P_j}{\partial \zeta}\right|_{\zeta=-1} \hat{T}_j \qquad \textbf{Eq.14}$$

In all, a system of N+1 equations for the N+1 unknown $\hat{T}_j$ is obtained.

Following Eq.12, the quantities G and F in the generalized Reynolds equation (Eq.1) can be simplified by using the polynomial coefficients of the fluidity $\widehat{\xi_{F\,j}}$. The development of the Dowson integrals (Eq.3) following the coordinate transformation is detailed in [3] and [4].

$$G = -\frac{\rho h^3}{12}\left(\widehat{\xi_{F\,0}} + \frac{2}{5}\widehat{\xi_{F\,2}} - \frac{\widehat{\xi_{F\,1}}^{\,2}}{3\widehat{\xi_{F\,0}}}\right);\;\; F = \rho h\left(\frac{\widehat{\xi_{F\,0}}}{2} - \frac{\widehat{\xi_{F\,1}}}{6}\right) \qquad \textbf{Eq.15}$$

2.4 Numerical scheme and resolution

Finite volume method is used to discretize the energy and the Reynolds equations. For stability reasons, the temperature at the face cells is approximated using the upwind discretization scheme. The coupled system of equations (Reynolds equation and energy equation) are solved in a sequential way.

3 Validation and discussion

The current numerical approach was validated by confrontations with 3 test cases published in the literature. The first case is an infinite inclined slider bearing. The LPCM is validated by comparing the numerical solution to the reference results obtained by Elrod. In the meantime, this case shows also the efficiency of LPCM compared to NDM in terms of computational time. The second case uses a parabolic slider to validate the cavitation models. The third and last case compares the pressure and the temperature measured in a two-lobe journal bearing with the predictions of the present solver.

3.1 The inclined 1D slider bearing

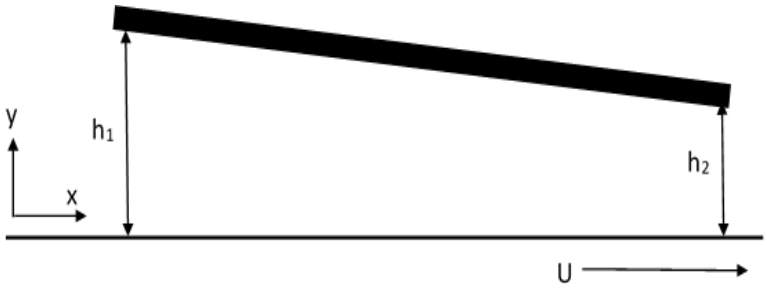

Figure 1 Geometry of the 1D slider

The new solver is applied to predict pressure and temperature of an oil lubricated 1D infinite slider presenting a linearly decreasing film thickness varying from $h_1 = 182.88\ \mu m$ to $h_2 = 91.44\ \mu m$

(Figure 1). The top wall is stationary while the bottom wall has a constant velocity $U = 31.946\, m/s$. The density of the lubricant is $\rho = 800$ kg/m^3, the specific heat capacity $C_p = 2.0\, kJ \cdot kg^{-1} \cdot K^{-1}$ and the thermal conductivity $\lambda = 0.14\, W \cdot m^{-1} \cdot K^{-1}$. The temperature-dependent viscosity follows an exponentially decaying law $\mu(T) = 0.13885e^{-0.045(T-20.0)}$. The computational domain is discretized using 30 control volumes (CV) in the main flow direction and 10 Lobatto points across the film thickness.

Figure 2 depicts the pressure distribution along the main flow direction. The pressure predicted by the current model shows good agreement with the results published by Elrod [2]. Figure 3 presents the variation across the film thickness of the outlet temperature. Again, the predictions of the current model show good agreement with [2].

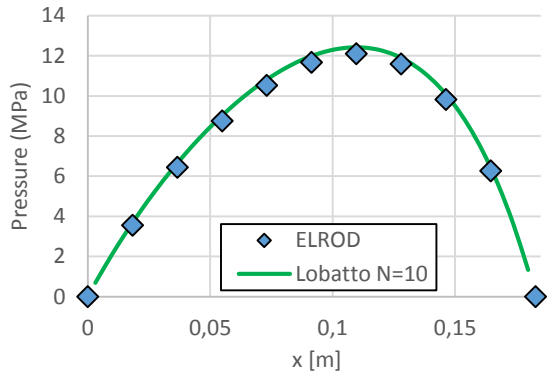

Figure 2: Pressure distribution

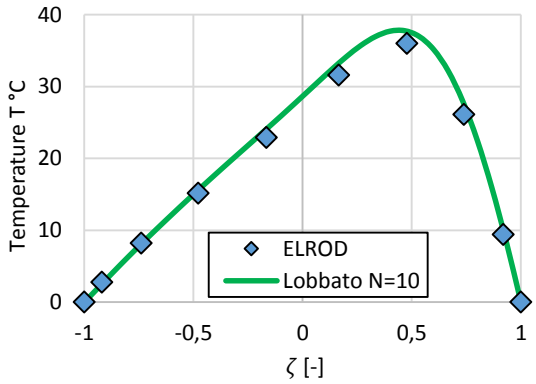

Figure 3: Outlet temperature distribution across the fluid film

This 1D inclined slider is also used to compare the efficiency of the LPCM compared to the NDM. Since LPCM reduces the number of the overall system unknowns, it is necessary to carry out a grid dependent test for the NDM prior to any efficiency comparison. Seven different grid refined in the y direction are used (10, 20, 40, 60, 80, 100, and 120 equally spaced CV) while the number of control volumes is kept fixed in the x direction and equal to 30. The relative error between two successive grids in terms of wall temperature gradients is defined as:

$$\varepsilon_K(y = 0\ or\ h) = \frac{\sqrt{\frac{1}{n}\sum_{i=1}^{n}\left(\frac{\partial T_K(x_i,y)}{\partial y} - \frac{\partial T_{K+1}(x_i,y)}{\partial y}\right)^2}}{\sqrt{\frac{1}{n}\sum_{i=1}^{n}\left(\frac{\partial T_{K+1}(x_i,y)}{\partial y}\right)^2}} \qquad \textbf{Eq.16}$$

where $n = 30$ is the number of CVs in x direction and K is the grid refinement level in the y direction.

Figure 4 shows that 40 CVs in y direction are necessary to reach a satisfactory mesh-independent solution while keeping a reasonable computational cost (Figure 5). Thus, the solution obtained by NDM with 40 equally spaced CVs over the film thickness is considered as the reference.

Figures 6 and 7 present the variation of the temperature gradient at the walls along the main flow direction (x direction) for different number of Lobatto points. The aforementioned figures show that 9 Lobatto points are sufficient to reach a good agreement with the results obtained by the NDM with 40 equally spaced CVs (considered as the reference).

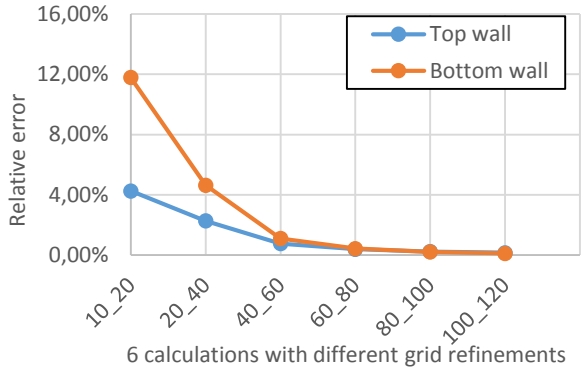

Figure 4: Relative error in function of the grid refinements

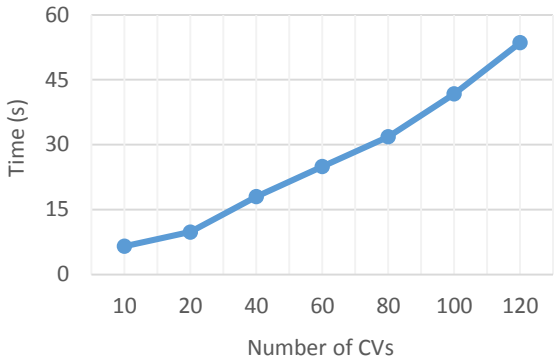

Figure 5: Computational time of NDM in function of number of y direction CVs

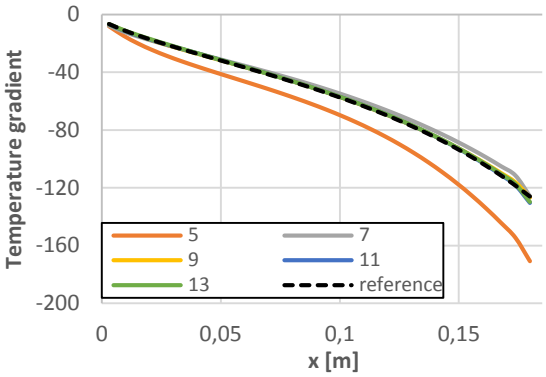

Figure 6: Temperature gradient at the top wall with different number of Lobatto points

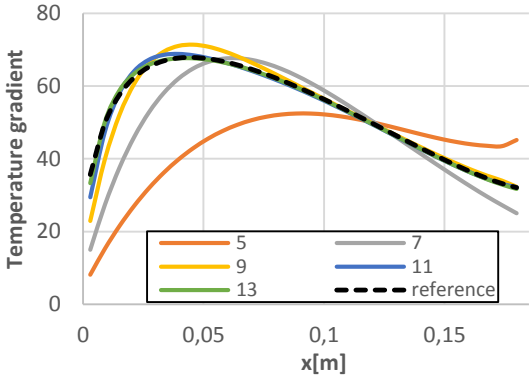

Figure 7: Temperature gradient at the bottom wall with different number of Lobatto points

The relative error between the reference temperature gradients at the walls (obtained using NDM) and the ones predicted by using N Lobatto points is defined as:

$$\varepsilon_{N_{Lobatto}}(\zeta = -1 \; or \; 1) = \frac{\sqrt{\frac{1}{n}\sum_{i=1}^{n}\left(\frac{\partial T_{N_{Lobatto}}(x_i,\zeta)}{\partial \zeta} - \frac{\partial T_{reference}(x_i,\zeta)}{\partial \zeta}\right)^2}}{\sqrt{\frac{1}{n}\sum_{i=1}^{n}\left(\frac{\partial T_{reference}(x_i,\zeta)}{\partial \zeta}\right)^2}} \qquad \textbf{Eq.17}$$

where $\zeta = 1 \; or \; \zeta = -1$, $n = 30$ is number of CVs in x direction

$\frac{dT_{N_{Lobatto}}}{d\zeta}$: temperature gradient obtained by LPCM with N Lobatto points

$\frac{dT_{reference}}{d\zeta}$: reference temperature gradient obtained by NDM with 40 CVs across the film thickness.

Figure 8 depicts the variation of the relative error (Eq.17) with the number of Lobatto points. The relative error drops rapidly and remains below 2% starting from 11 Lobatto points. Figure 9 shows that the computational time for the LPCM does not exceed 2 seconds while the reference method takes about 18 seconds. The economy of computational time brought by the LPCM approach is important.

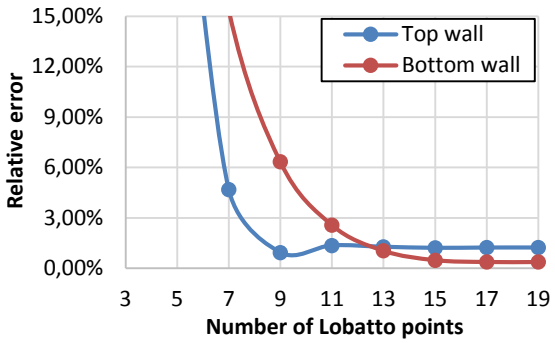

Figure 8: Relative error between LPCM and NDM versus the number of Lobbato points

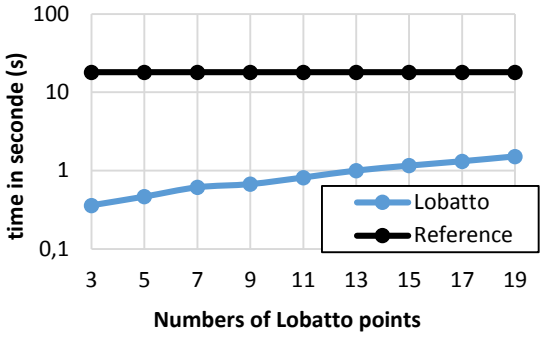

Figure 9: Computational time in function of numbers of Lobatto points.

3.2 The parabolic 1D slider

A parabolic 1D slider proposed by Vijayaraghavan and Keith [8] in 1989 was used to validate the cavitation models. The slider length is 76.2 mm, the minimum and maximum film thickness are 25.4µm and 50.8µm, the sliding speed is U = 4.57m/s and the atmospheric pressure is imposed at the inlet and outlet. The lubricant viscosity is constant and equal to $0.039\ Pa \cdot s$. The comparison of two cavitation approaches (ACM and FBNS) with the published reference results from [8] is shown in Figure 10.

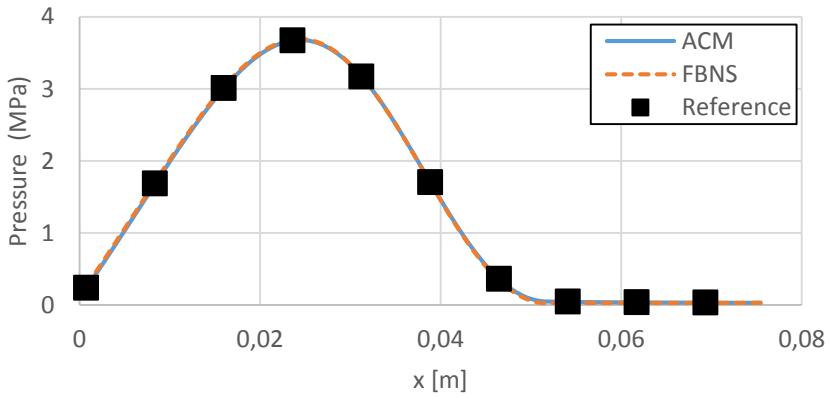

Figure 10: Comparison of pressure distribution obtained by different models for the parabolic slider

3.3 Journal bearing with axial groove

A recent experimental work was published by Giraudeau et al. [10] in 2016 to analyze the effect of geometrical discontinuities in the case of a two-lobe journal bearing with an axial supply groove. The tested bearing length is 68.4 mm and its diameter is 100 mm. The radial assembly clearance is 68 μm while the radial bearing clearance is 143 μm. The bearing is lubricated using an ISO VG 46 oil supplied at a constant pressure of 0.17 MPa and at a constant temperature of 43°C. For the calculation, the following oil characteristics are used: $\rho = 850\ kg/m^3$, $C_p = 2000$ J/kg/K and λ =0.13 W/m/K. The viscosity of the oil is 0.0416 Pa.s at 40°C and 0.0191 Pa.s at 60°C. The variation is described by an exponentially decaying law similar to Eq.9.

Three operating conditions (500 rpm and 10kN load, 2000 rpm and 8kN load and 3500 rpm and 6kN load) are used for comparisons. The shaft is considered to have a constant temperature estimated from experiments (Dirichlet boundary condition) while adiabatic wall conditions are imposed on the bushing (Neumann boundary condition). The computational domain is discretized using 32×16 CVs in circumferential and axial directions while 11 Lobatto points are used to describe the temperature variation across the fluid film. Results are shown only for the loaded lobe (i.e lower lobe) where the

thermal effects are more important. Figures 11-16 depict the pressure and the temperature variation in the circumferential direction. The predicted pressures show good agreement with the measurements. The predicted temperature shows a reasonable agreement with the measurements and the quality of the prediction could be improved if the thermo-deformation of the bushing is considered and the thermal boundary conditions for the energy equation are refined.

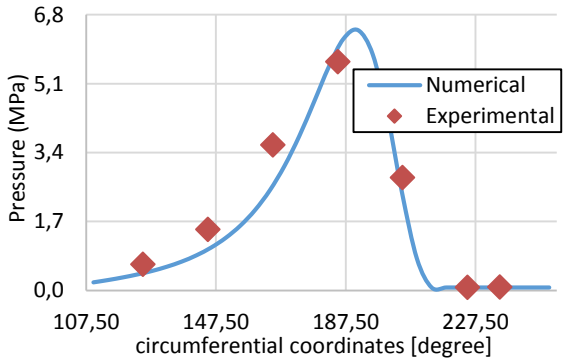

Figure 11: Comparison of measured pressures and current THD solver (500 rpm, 10kN load)

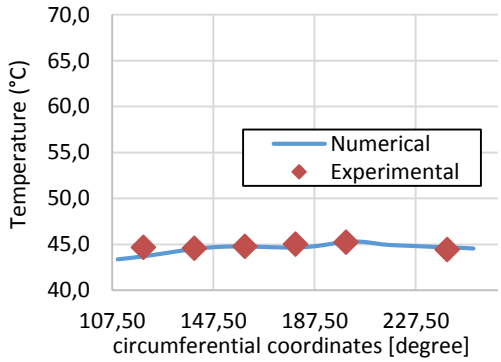

Figure 12: Comparison of measured temperatures and current THD solver (500 rpm, 10kN load)

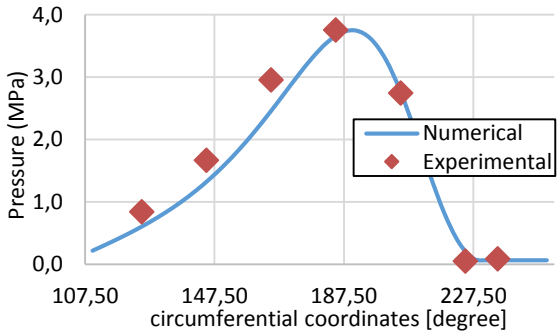

Figure 13: Comparison of measured pressures and current THD solver (2000 rpm, 8kN load)

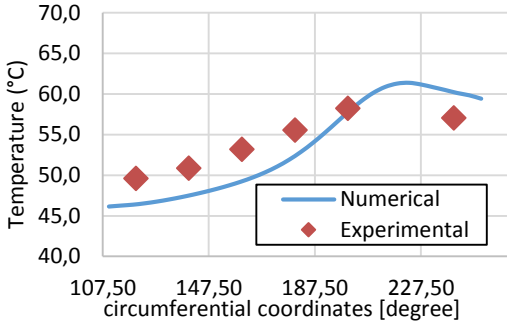

Figure 14: Comparison of measured temperatures and current THD solver (2000 rpm, 8kN load)

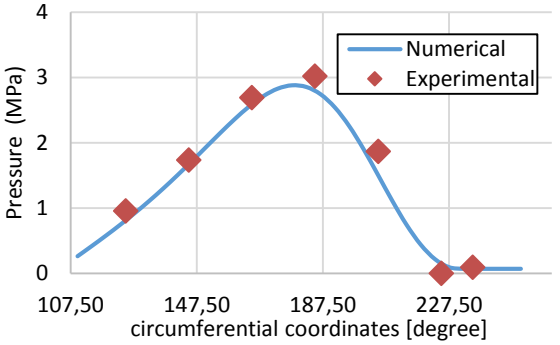

Figure 15: Comparison of measured pressures and current THD solver (3500 rpm, 6kN load)

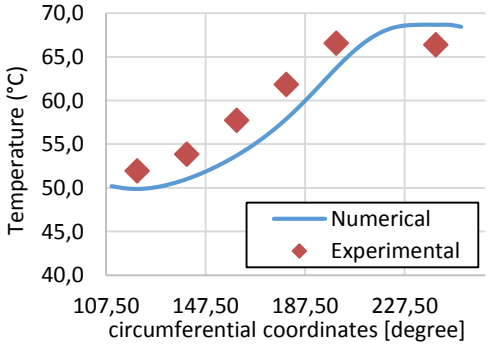

Figure 16: Comparisons of measured temperatures and current THD solver (3500 rpm, 6kN load)

4 Conclusion and prospective

An efficient numerical solver for thermo-hydrodynamic analysis of journal bearing in steady state regime was developed using LPCM. This spectral method provides an important reduction of the calculation time and can be coupled with cavitation algorithms to perform THD analyses of journal

bearings. Two cavitation algorithms were integrated in the present solver to take into account the film rupture and reformation. Finally, the numerical solver was validated against numerical and experimental data from the literature. Even though the thermal deformation of the bushing is not considered, the numerical results showed reasonable agreement with the experimental data. However, a thermo-elastic-hydrodynamic analysis is necessary and planned to be performed in order to obtain a refined numerical solution. Furthermore, the transient regime will be integrated in the solver.

Nomenclature

x	coordinate in the x direction [m]	β	coefficient of cavitation model [-]
y	coordinate in the y direction [m]	u	velocity field in the x direction [m s^{-1}]
z	coordinate in the z direction [m]	v	velocity field in the y direction [m s^{-1}]
ζ	coordinate transformation in y direction [-]	w	velocity field in the z direction [m s^{-1}]
p	Pressure [Pa]	T	Temperature [°C]
h	Film thickness [m]	C_p	specific heat capacity [J kg^{-1} °C^{-1}]
ρ	Density [kg m^{-3}]	λ	thermal conductivity [W m^{-1} °C^{-1}]
ξ	parameter of integration	$\widehat{\xi_{F\,j}}$	polynomial coefficients of fluidity
μ	dynamic viscosity [Pa.s]	P_j	Legendre polynomial
U	velocity of mobile slider [m s^{-1}]	$\hat{T}_j$	polynomial coefficients of temperature
θ	Filling fraction in cavitation models	ϕ_q	temperature gradient [°C m^{-1}]
p_{cavi}	cavitation pressure	ξ_F	fluidity [Pa^{-1} s^{-1}]

References

[1] Elrod HG, Brewe DE. "Thermo hydrodynamic analysis for laminar lubricating films", Technical report, NASA technical memorandum 88845, 1986

[2] Elrod HG. "Efficient numerical method for computation of thermo hydrodynamics of laminar lubricating films", Technical report, NASA Lewis Research Center, 1989.

[3] Moraru LE. "Numerical prediction and measurements in the lubrication of aeronautical engine and transmission components" [PhD.thesis]. University of Toledo, 2005.

[4] Feng K, Kaneko S. "Thermohydrodynamic study of multiwound foil bearing using Lobatto point quadrature", ASME Journal of Tribology, Vol.131, April 2009

[5] Mahner M, Lehn A, Schweizer B, "Thermogas and thermohydrodynamic simulation of thrust and slider bearings: Convergence and efficiency of different reduction approaches", Tribology International, pp 539-554, 2016

[6] Elrod HG, "A cavitation algorithm", ASME Journal of Lubrication Technology, 1981, Vol. 103, pp.350-354

[7] Woloszynski T, Podsiadlo P, Stachowiak GW, "Efficient Solution to the Cavitation Problem in Hydrodynamic", Tribology Letters, Springer, 2015

[8] Vijayaraghavan D. and Keith Jr. T. G. "Development and Evaluation of a Cavitation Algorithm", Tribology Transactions, 32:2, 225-233, 1989

[9] D. Bonneau, A. Fatu, D. Souchet, "Paliers hydrodynamiques1 and 2, équations, modèles numériques isothermes et lubrification mixte, Lavoisier, Paris, 2011

[10] Giraudeau.C, "Influence des discontinuités géométriques sur les performances des paliers en régime thermoélastohydrodynamique (TEHD) " [PhD.thesis], University de Poitiers, 2016.